

# State Switching of Terahertz Reflection and Orbital Angular Momentum in Phase Change Metasurfaces

Changqing Li<sup>ID</sup>, Canhui He, and Zhengyong Song<sup>ID</sup>

**Abstract**—Metasurfaces with dynamically switchable functions have received extensive attention, and are in high demand in various applications. In this work, dynamically switchable metasurfaces are proposed based on phase change material-vanadium dioxide. They consist of vanadium dioxide blocks, silicon dioxide spacer, and gold film. By changing the size of vanadium dioxide block, vanadium dioxide in the metallic state forms a gradient metasurface. A specially arranged gradient metasurface is designed to achieve a 360° phase modulation capability. Normally incident plane wave is reflected to the right side at the angle of 36.9° at 2.5 THz. When vanadium dioxide switches from the metallic state to the insulating state, the switching of anomalous reflection and specular reflection is realized. In addition, when vanadium dioxide is metal, a vortex beam generator is implemented to generate orbital angular momentum beams with  $l = 1$  and  $l = 2$ . The number of orbital angular momentum mode can be switched from  $l = 0$  to  $l = 1$  or  $l = 2$  by changing the state of vanadium dioxide. Since the structure of meta-atom is a square block, the design is simple and easy to integrate. At the same time, the switchable function is accurately implemented without side lobe. The proposed design has potential applications in terahertz switching and communication.

**Index Terms**—Metasurface, vanadium dioxide, anomalous reflection, orbital angular momentum.

## I. INTRODUCTION

ACHIEVING full control on electromagnetic wave is greatly significant. It has urgent needs in the fields of communication, energy, national defense, and so on. However, the ability of traditional natural materials to control electromagnetic wave is limited, which hinders the development of electromagnetic device. Metamaterials are specially designed subwavelength microstructures. According to requirements, artificial meta-atoms are designed and then combined in a special arrangement. Metamaterials are used to build devices that effectively control amplitude, phase, polarization, and wavefront of electromagnetic wave. Therefore, metamaterials have received extensive attention from scientific and engineering communities for their unprecedented control over electromagnetic wave at the subwavelength scale. By appropriately controlling the properties

Manuscript received June 13, 2022; accepted June 13, 2022. Date of publication June 16, 2022; date of current version June 27, 2022. This work was supported by the National Natural Science Foundation of China under Grant 11974294. (*Corresponding author: Zhengyong Song.*)

The authors are with the National Innovation Platform for the Fusion of Industry and Education in Integrated Circuits, School of Electronic Science and Engineering, Xiamen University, Xiamen, Fujian 361005, China (e-mail: 36620211150344@stu.xmu.edu.cn; 36620211150337@stu.xmu.edu.cn; zhysong@xmu.edu.cn).

Digital Object Identifier 10.1109/JPHOT.2022.3183569

of electromagnetic wave, many novel physical phenomena and interesting applications are obtained. Examples include negative refraction [1]–[3], invisible cloak [4]–[6], and perfect lens [7]–[9].

Recently, metasurfaces have become a hot topic of research. They are two-dimensional metamaterials that combine artificial electromagnetic microstructures in spatial order. Metasurfaces, as a planar version of metamaterials, have realized many new phenomena of electromagnetic wave regulation that cannot be achieved by three-dimensional bulk metamaterials. It uses the abrupt effect on the interface to achieve the control of electromagnetic wave. This improves efficiency and reduces loss of electromagnetic wave. Metasurfaces are simple to fabricate, easy to integrate, and provide solutions for on-chip applications. Gradient metasurfaces are formed by gradient phase distribution. Some applications of gradient metasurfaces are proposed. In 2016, N. M. Estakhri *et al.* investigated theoretical limitations and potentials of passive gradient metasurfaces to manipulate arbitrary wave [10]. Unlike similar metasurfaces using traditional ray-optics method, the extreme-angle wave-bending metasurface they employed significantly improved the overall efficiency by 30%. In 2017, Y. Li *et al.* carried out theoretical analysis and experimentally verified asymmetric wave transmission in lossy acoustic gradient-index metasurface [11]. In 2018, J. Li *et al.* designed three refractive metasurfaces. These metasurfaces are capable of anomalous reflection, redirecting normally incident plane waves to 60°, 70°, and 80° on transmission [12]. The efficiency of the bianisotropic design exceeds 90%, while the corresponding generalized Snell's law based design is well below this value. In 2020, H. Kazemi *et al.* introduced a chiral gradient metasurface to achieve redirection of transmission and perfectly rotate the polarization of the refracted wave [13]. Their results showed that plane wave at normal incidence is deflected by 45° as a refracted plane wave with a power efficiency of 72%, accompanied by a 90° polarization rotation. In addition, vortex beam carrying orbital angular momentum (OAM) can be generated by spiral phase distribution. In 2016, D. Hakobyan *et al.* reported on the fabrication and characterization of optical vortex generators made of metallic metasurfaces [14]. In 2018, Y. Shen *et al.* presented a metasurface-based reflective-type approach to form a nondiffractive Bessel beam carrying OAM [15]. The prototype integrated the planar feeding source with the metasurface. In 2019, M. R. Akram *et al.* designed a novel bilayer meta-atom with a periodic unit cell-based transmission efficiency of up to 85% [16]. These meta-atoms were then used to construct metasurfaces that generate vortex beams carrying

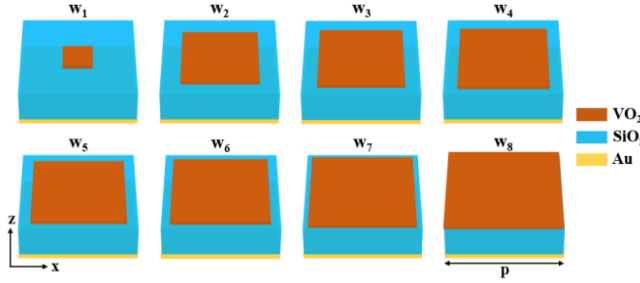


Fig. 1. 3D schematic diagram of the designed eight different meta-atoms. The dimensions are  $w_1 = 6.5 \mu\text{m}$ ,  $w_2 = 16.8 \mu\text{m}$ ,  $w_3 = 18.5 \mu\text{m}$ ,  $w_4 = 19.4 \mu\text{m}$ ,  $w_5 = 20.2 \mu\text{m}$ ,  $w_6 = 21.2 \mu\text{m}$ ,  $w_7 = 22.8 \mu\text{m}$ , and  $w_8 = 25 \mu\text{m}$ .

OAM. In 2020, B. Liu *et al.* proposed a concept of multifunctional vortex beam [17]. It is realized by a dynamic reflective metasurface which is capable of controlling vortex beam spatiotemporally.

Vanadium dioxide ( $\text{VO}_2$ ) is an excellent tunable material. It has special phase transition properties.  $\text{VO}_2$  is an insulator with a monoclinic crystal structure at room temperature. Once phase transition temperature is exceeded,  $\text{VO}_2$  changes into tetragonal rutile crystal and acts as a metal. This insulator-to-metal transition is fastly achieved by applying thermal, electrical, or optical stimulus. This structural transition leads to significant changes in electrical and optical properties of  $\text{VO}_2$ . The conductivity of  $\text{VO}_2$  increases by several orders of magnitude during the transition. Up to now, research on  $\text{VO}_2$ -based devices has involved many aspects, such as optical switch [18]–[20], absorber [21]–[23], and filter [24]–[26]. In 2018, M. Sun *et al.* proposed a photonic switch based on  $\text{VO}_2$  material, whose structure is composed of an array of hexagonal nanoholes [27]. It achieves a maximum transmission rate of 37% at optical communication band. In 2020, M. Zhang *et al.* designed a terahertz absorber composed of a graphene-spacer- $\text{VO}_2$ -spacer-metal structure with narrowband and broadband properties [28]. A band of 100% absorption is reached at 1.37 THz. In the frequency range of 1.05–2.35 THz, broadband absorption is formed with absorption >90%. In 2021, Z. Che *et al.* presented a controllable terahertz filter with dual narrowband characteristics, and its structure consists of two n-shaped waveguides and one  $\text{VO}_2$  defect [29]. Switching between passband and stopband is achieved at 1.287 THz and 1.447 THz. The proposed filter has great application prospects in the field of temperature-controlled switches in integrated photonic circuits.

In this work, switchable metasurfaces are designed by exploiting the special properties of phase change material  $\text{VO}_2$ . By arranging  $\text{VO}_2$  blocks with different sizes, eight meta-atoms are designed. When  $\text{VO}_2$  is in the metallic state, the metasurface formed by eight meta-atoms achieves phase coverage of 0–360°. Dynamically switchable gradient metasurface and vortex beam generator are presented. At the frequency of 2.5 THz, plane wave under normal incidence is anomalously reflected at 36.9°, and this behavior is independent of polarization. The designed vortex beam generators generate OAM beams with  $l = 1$  and  $l = 2$ . When  $\text{VO}_2$  changes from the metallic state to the insulating state, anomalous reflection switches to specular reflection. And

the beam generated by vortex beam generator switches from  $l = 1$  or  $l = 2$  to  $l = 0$ . Different from circularly polarized wavefront control [30], this work is mainly applied to wavefront control on linearly polarized wave. Although many works on gradient metasurface have been proposed [31], there are still few studies on  $\text{VO}_2$ -based reconfigurable metasurface. Compared with [32], our design achieves phase coverage of 360° with phase difference 45° between adjacent meta-atoms, and realizes the desired function without side lobe.

## II. DESIGN AND METHOD

Three-dimensional schematic diagram of the designed switchable meta-atoms is shown in Fig. 1. The designed metasurfaces consist of eight meta-atoms with different  $\text{VO}_2$  block sizes. Each meta-atom is composed of three parts: the top  $\text{VO}_2$  block, the middle silicon dioxide spacer, and the bottom gold film. The period of meta-atom is  $P = 25 \mu\text{m}$ . The thicknesses of  $\text{VO}_2$  blocks, silicon dioxide spacer, and gold film are 1  $\mu\text{m}$ , 6  $\mu\text{m}$ , and 1  $\mu\text{m}$ , respectively. The dimension of  $\text{VO}_2$  blocks changes from  $w_1$  to  $w_8$ . Electromagnetic simulation of the proposed switchable metasurface is carried out with the help of finite element method (commercial software-Comsol Multiphysics). Periodic boundary conditions are used for calculating unit cell along x and y directions, and linear plane wave shines structure from z direction. Adaptive mesh refinement is adopted, which helps to ensure the convergence of the simulated results. Silicon dioxide acts as a dielectric layer with relative dielectric permittivity of 3.85 [33], [34]. The bottom gold film is assumed as a lossy metal with the conductivity of  $4.561 \times 10^7 \text{ S/m}$ . Dielectric permittivity of  $\text{VO}_2$  in the terahertz range is described by Drude model  $\varepsilon(\omega) = \varepsilon_\infty - \frac{\omega_p^2}{\omega^2 + i\omega\gamma}$  [35]–[37]. In the above equation,  $\varepsilon_\infty = 12$  is dielectric permittivity at the infinite frequency,  $\omega_p$  is plasma frequency dependent on conductivity, and  $\gamma = 5.75 \times 10^{13} \text{ s}^{-1}$  is collision frequency. When  $\text{VO}_2$  is in the metallic (insulating) state, the conductivity is  $2 \times 10^5 \text{ S/m}$  (200 S/m) and its  $\omega_p$  is  $1.143 \times 10^{15} \text{ rad/s}$  ( $3.6149 \times 10^{13} \text{ rad/s}$ ). Phase transition process of  $\text{VO}_2$  is stimulated by optical pumping [38], [39].

## III. RESULTS AND DISCUSSIONS

The overall functional behavior of metasurface arises from the superposition of wavefronts of different meta-atoms. Therefore, ensuring 360° phase coverage is a key point in the design. Reflection coefficient should also be maintained at a certain level to ensure efficiency. To achieve arbitrary manipulation of the reflected wavefront, eight different meta-atoms are designed. In simulation, the reference plane is set on the top of  $\text{VO}_2$  block. Simulated results are shown in Fig. 2. When  $\text{VO}_2$  is in the metallic state, phase range increases from –135° to 180° as the size of  $\text{VO}_2$  block changes. At the target frequency of 2.5 THz, the designed eight meta-atoms achieve phase coverage of 0–360°, and phase difference between two adjacent cells is stable around 45°. Reflection amplitude of eight meta-atoms remains above 0.65, which ensures a certain reflection efficiency. This result verifies that reflection phase is effectively modulated

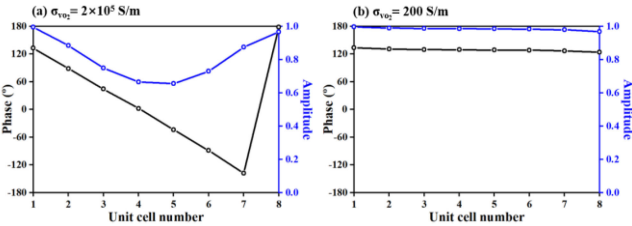


Fig. 2. Reflection phases (black) and amplitudes (blue) of eight meta-atoms with y-polarized wave under normal incidence for  $\sigma_{VO_2} = 2 \times 10^5 \text{ S/m}$  (a) and  $\sigma_{VO_2} = 200 \text{ S/m}$  (b) at 2.5 THz.

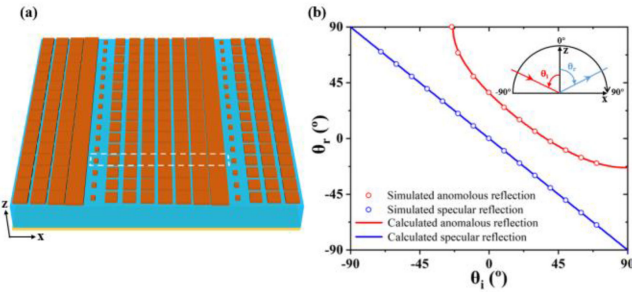


Fig. 3. (a) Structural diagram of the designed gradient metasurface. Gradient metasurface has different beam steering functions under different VO<sub>2</sub> states. (b) Simulated and calculated results of reflection angles with different incident angles in two states.

by changing VO<sub>2</sub> block size. However, when VO<sub>2</sub> is in the insulating state, no matter how to change the size of VO<sub>2</sub> block, it has little effect on the fluctuation of phase and amplitude. It is the characteristic of VO<sub>2</sub>, a phase change material, that enables the realization of switchable metasurface.

#### A. Gradient Metasurface

As shown in Fig. 3(a), eight meta-atoms are combined along the x-axis in order of decreasing phase to form a supercell. To simulate deflection effect, eight supercells are set along x direction, and periodic boundary conditions are set along y direction. Electromagnetic wave is incident at different angles relative to z axis. According to the generalized Snell's law, metasurface with a certain phase gradient can be formed by an array of scatterers with subwavelength spacing. The designed gradient metasurface theoretically creates an additional wave vector and changes the wavefront of the reflected beam. The structure of meta-atom is square, thus enabling beam steering. In the defined coordinate system (the inset in Fig. 3(b)), reflection angle  $\theta_r$  is derived as  $\theta_r = \sin^{-1}(-\sin \theta_i + \xi/k_0)$ , where  $\theta_i$  is incident angle,  $\xi = \frac{2\pi}{8P}$  is the gradient value, and  $k_0 = \frac{2\pi}{\lambda}$  is the wavevector at wavelength  $\lambda$  [40]. Therefore, by theoretical calculation, two results are obtained. When phase gradient is zero, the calculation shows  $\theta_r = -\theta_i$ , which is the phenomenon of specular reflection (blue curve in Fig. 3(b)). When VO<sub>2</sub> switches from the insulating state to the metallic state, phase gradient is formed. The relationship between  $\theta_r$  and  $\theta_i$  is obtained by substituting period P and wavelength  $\lambda$  corresponding to 2.5 THz into the above formula. The calculated result of anomalous reflection is shown in the red curve in Fig. 3(b). In order to verify the reliability of the switchable function of anomalous reflection and specular reflection, a series of incident angles are selected for

simulation. Simulated results are shown in Fig. 3(b), red circles and blue circles represent the relationship between  $\theta_r$  and  $\theta_i$  of anomalous reflection and specular reflection, respectively. Obviously, simulated results are in good agreement with calculated curves. It is demonstrated that the designed gradient metasurface can dynamically switch between two functions of anomalous reflection and specular reflection. In addition, there is a critical angle  $\theta_{ic} = \sin^{-1}(-\sin 90^\circ + \xi/k_0)$  for  $\theta_i$  such that as  $|\theta_i| > |\theta_{ic}|$ , the reflected beam becomes a surface wave bounded on the metasurface which cannot radiate to free space [41].

In the above results, three special incident angles are selected for analysis in the far-field scattering patterns. As shown in Fig. 4, far-field scattering patterns of the reflected beams in different VO<sub>2</sub> states exhibit different phenomena at the incident angles of 0°, 17.5°, and 36.9°. In Fig. 4(a), when plane wave is incident vertically ( $\theta_i = 0^\circ$ ), it is anomalously reflected at reflection angle  $\theta_r = 36.9^\circ$ . When VO<sub>2</sub> switches to the insulating state, the reflected beam in Fig. 4(d) is reflected out in the form of specular reflection with  $\theta_r = 0^\circ$ . The anomalously reflected beam has no other high-intensity side lobes, and the intensity reaches more than half of the specularly reflected beam. Through calculation in Fig. 4(b), we get the special negative reflection phenomenon of  $\theta_r = \theta_i$  when  $\theta_i = 17.5^\circ$ . The obliquely incident beam returns along the original path. And it is switched to positive reflection ( $\theta_r = -17.5^\circ$ ) in Fig. 4(e). In Fig. 4(c), when  $\theta_i = 36.9^\circ$ , the anomalously reflected beam is perpendicular to the metasurface ( $\theta_r = 0^\circ$ ). The result in Fig. 4(f) is still in the form of specular reflection.

#### B. Vortex Beam Generator

In 1992, L. Allen *et al.* firstly confirmed that a light beam can carry OAM [42]. The realization of vortex beam carrying OAM through metasurface has become a research hotspot. OAM waves have applications in optical, terahertz, and microwave regions. Among them, the use of OAM in wireless communication to improve channel capacity has great application value [43]. Phase distribution of OAM wave is described by  $e^{il\theta}$ , where  $l$  is OAM mode number and  $\theta$  is azimuth angle. The well-known spin angular momentum (SAM) has a fixed state with linear and circular polarizations of  $s = 0$  and  $s = \pm 1$ , respectively. OAM provides an infinite number of orthogonal states. OAM mode number can be  $l = 0, \pm 1, \pm 2, \pm 3 \dots$ , where wavefront phase of  $l = 0$  vortex beam is uniform. When  $l$  is a non-zero integer, vortex beam has a spiral phase distribution.

To realize vortex beam generator producing OAM wave, two metasurfaces composed of eight meta-atoms are designed in Fig. 5. Space and reflection phase are discretized, and the metasurfaces with  $48 \times 48$  meta-atoms are divided into distinct regions. Perfect matched layers are set along x and y directions. Phase difference of each region is 45°. For  $l = 1$ , the metasurface is divided into eight regions, and for  $l = 2$ , the metasurface is divided into sixteen regions. Eight kinds of meta-atoms are arranged in the corresponding area in the  $xoy$  plane, and plane wave is incident on the metasurface along z direction for simulation and observation.

Simulated results of far-field scattering patterns are shown in Fig. 6 ( $l = 1$ ) and Fig. 7( $l = 2$ ). The results show that

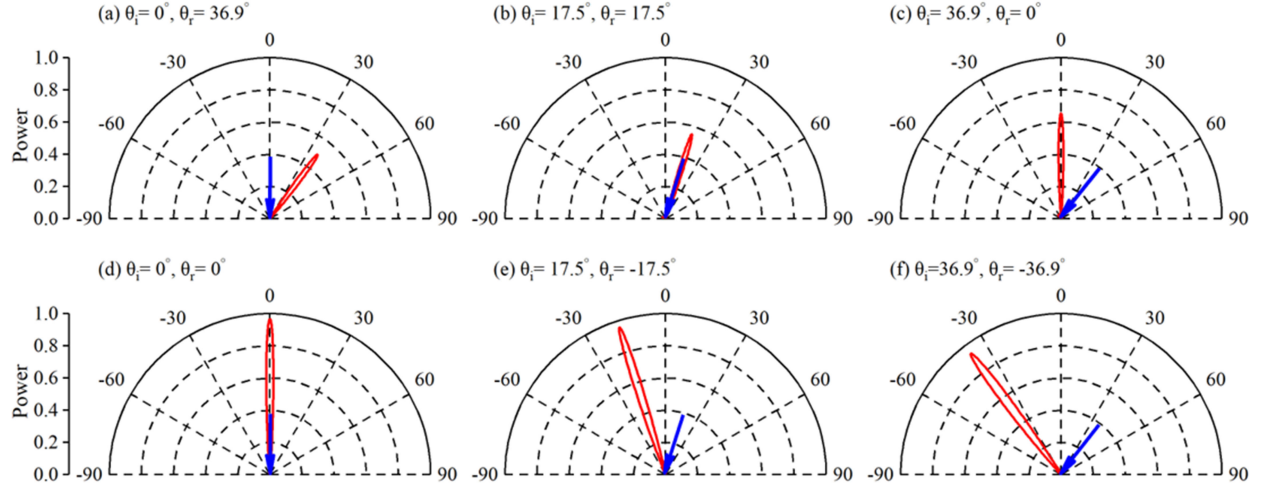


Fig. 4. Simulated deflection angle and power of the reflected beam (red curve) at 2.5 THz. Incident wave is polarized along y direction. Blue arrows only indicate the direction of incidence. (a)–(c) are far-field scattering patterns with  $\sigma_{VO_2} = 2 \times 10^5$  S/m. (d)–(f) are far-field scattering patterns with  $\sigma_{VO_2} = 200$  S/m.

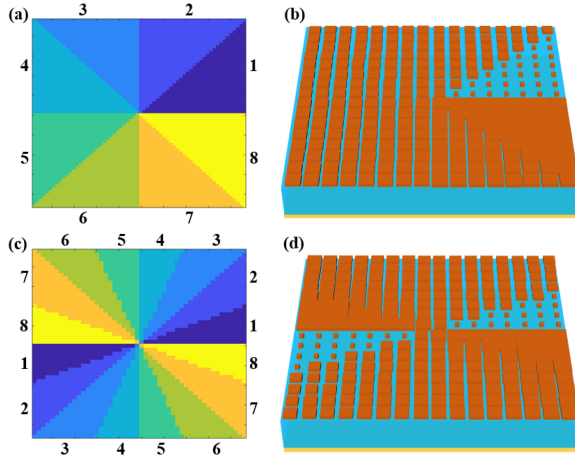


Fig. 5. Spatial distribution of the proposed metasurface consisting of eight regions 1–8 representing by different colors in (a)  $l = 1$  and (c)  $l = 2$ . Part of the simulated metasurface for generating OAM  $l = 1$  (b) and  $l = 2$  (d).

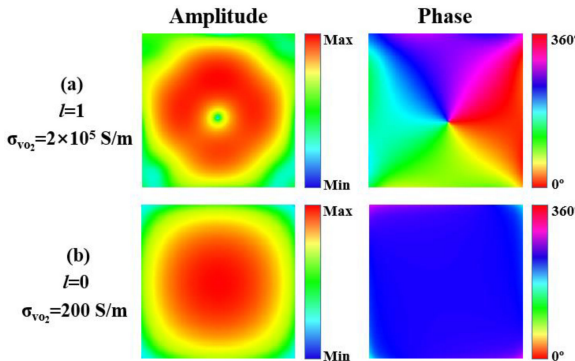


Fig. 6. Simulated far-field patterns in different OAM modes for  $\sigma_{VO_2} = 2 \times 10^5$  S/m,  $l = 1$  (a) and  $\sigma_{VO_2} = 200$  S/m,  $l = 0$  (b).

when  $\sigma_{VO_2} = 2 \times 10^5$  S/m, the designed metasurface forms a vortex beam carrying OAM. Amplitude of OAM is a ring-shaped intensity distribution with a deep null region at the center. For  $l = 2$ , the central area is split into two null points. Neither amplitude

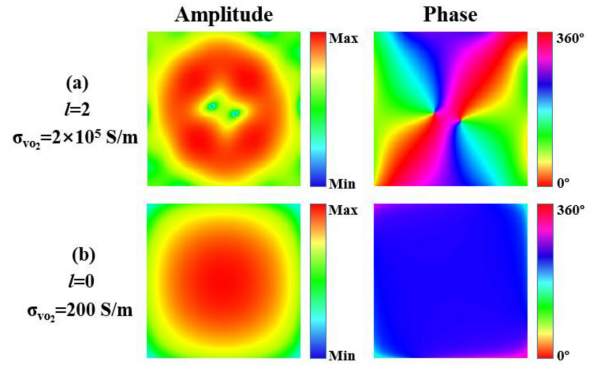


Fig. 7. Simulated far-field patterns in different OAM modes for  $\sigma_{VO_2} = 2 \times 10^5$  S/m,  $l = 2$  (a) and  $\sigma_{VO_2} = 200$  S/m,  $l = 0$  (b).

of  $l = 1$  nor amplitude of  $l = 2$  are completely uniform. This is due to the finite size of the metasurface and the discrete phase distribution in vortex generator. Phase results of OAM show a  $360^\circ$  phase rotation for  $l = 1$  in Fig. 6(a) and a  $720^\circ$  phase rotation for  $l = 2$  in Fig. 7(a). The generation of OAM with modes  $l = 1$  and  $l = 2$  is confirmed from both amplitude and phase profiles. When  $\sigma_{VO_2} = 200$  S/m, the generated beams are plane wave with  $l = 0$  in Fig. 6(b) and Fig. 7(b), and its amplitude and phase distributions are completely uniform. The results in Fig. 6 and Fig. 7 show that vortex beam generator realizes the switching of OAM mode from  $l = 1$  and  $l = 2$  to  $l = 0$ . Phase change of  $VO_2$  disrupts the spiral phase distribution of meta-atoms. Consequently, the wavefront of OAM generator is reconstructed.

#### IV. CONCLUSION

To summarize, switchable metasurfaces are proposed, and they are capable of anomalous reflection and generation of OAM. By changing the size of  $VO_2$  block, eight meta-atoms are designed to achieve a phase range coverage of  $0$ – $360^\circ$ . Using the proposed meta-atoms through appropriate arrangement, gradient metasurface and vortex beam generator are designed.

The designed gradient metasurface achieves dynamic switching between anomalous reflection and specular reflection at the frequency of 2.5 THz. When  $\sigma_{VO_2} = 2 \times 10^5$  S/m, the proposed vortex beam generator excites terahertz wave carrying OAM modes  $l = 1$  and  $l = 2$ . OAM mode can be switched from  $l = 1$  or  $l = 2$  to  $l = 0$  by changing the state of VO<sub>2</sub>. Simulated results clearly tell that precise control of terahertz wavefront is realized for linearly polarized wave. Due to the characteristics of simple structure design and easy integration, the potential applications of the designed metasurfaces are anticipated for dynamic beam steering. Our work may pave new paths in dynamically switchable terahertz metasurfaces.

## REFERENCES

- [1] R. Zhu, X. N. Liu, G. K. Hu, C. T. Sun, and G. L. Huang, "Negative refraction of elastic waves at the deep-subwavelength scale in a single-phase metasmaterial," *Nature Commun.*, vol. 5, pp. 5510, Nov. 2014.
- [2] R. A. Shelby, D. R. Smith, and S. Schultz, "Experimental verification of a negative index of refraction," *Science*, vol. 292, no. 5514, pp. 77–79, Apr. 2001.
- [3] N. Kaina, F. Lemoult, M. Fink, and G. Lerosey, "Negative refractive index and acoustic superlens from multiple scattering in single negative metasmaterials," *Nature*, vol. 525, no. 7567, pp. 77–81, Sep. 2015.
- [4] S. Zhang, C. Xia, and N. Fang, "Broadband acoustic cloak for ultrasound waves," *Phys. Rev. Lett.*, vol. 106, no. 2, Jan. 2011, Art. no. 024301.
- [5] X. Ni, Z. J. Wong, M. Michael, Y. Wang, and X. Zhang, "An ultrathin invisibility skin cloak for visible light," *Science*, vol. 349, no. 6254, pp. 1310–1314, Sep. 2015.
- [6] M. Manjappa, P. Pitchappa, N. Wang, C. Lee, and R. Singh, "Active control of resonant cloaking in a terahertz MEMS metasmaterial," *Adv. Opt. Mater.*, vol. 6, no. 16, Aug. 2018, Art. no. 1800141.
- [7] C. Ma and Z. Liu, "Focusing light into deep subwavelength using metasubstrates immersion lenses," *Opt. Exp.*, vol. 18, no. 5, pp. 4838–4844, Mar. 2010.
- [8] Y. Li, B. Liang, X. Tao, X. Zhu, X. Zou, and J. Cheng, "Acoustic focusing by coiling up space," *Appl. Phys. Lett.*, vol. 101, no. 23, Dec. 2012, Art. no. 233508.
- [9] M. Qi, W. Tang, and T. J. Cui, "A broadband Bessel beam launcher using metasubstrate lens," *Sci. Rep.*, vol. 5, Jun. 2015, Art. no. 11732.
- [10] N. M. Estakhri and A. Alu, "Wave-front transformation with gradient metasurfaces," *Phys. Rev. X*, vol. 6, no. 4, Oct. 2016, Art. no. 041008.
- [11] Y. Li *et al.*, "Tunable asymmetric transmission via lossy acoustic metasurfaces," *Phys. Rev. Lett.*, vol. 119, no. 3, Jul. 2017, Art. no. 035501.
- [12] J. Li, C. Shen, A. Diaz-Rubio, S. A. Tretyakov, and S. A. Cummer, "Systematic design and experimental demonstration of bianisotropic metasurfaces for scattering-free manipulation of acoustic wavefronts," *Nature Commun.*, vol. 9, Apr. 2018, Art. no. 1342.
- [13] H. Kazemi, M. Albooyeh, and F. Capolino, "Simultaneous perfect bending and polarization rotation of electromagnetic wavefront using chiral gradient metasurfaces," *Phys. Rev. Appl.*, vol. 13, no. 2, Feb. 2020, Art. no. 024078.
- [14] D. Hakobyan, H. Magallanes, G. Seniutinas, S. Juodkazis, and E. Brasselet, "Tailoring orbital angular momentum of light in the visible domain with metallic metasurfaces," *Adv. Opt. Mater.*, vol. 4, no. 2, pp. 306–312, Feb. 2016.
- [15] Y. Shen, J. Yang, H. Meng, W. Dou, and S. Hu, "Generating millimeter-wave bessel beam with orbital angular momentum using reflective-type metasurface inherently integrated with source," *Appl. Phys. Lett.*, vol. 112, no. 14, Apr. 2018, Art. no. 141901.
- [16] M. R. Akram, M. Q. Mahmood, X. Bai, R. Jin, M. Premaratne, and W. Zhu, "High efficiency ultrathin transmissive metasurfaces," *Adv. Opt. Mater.*, vol. 7, no. 11, Jun. 2019, Art. no. 1801628.
- [17] B. Liu, Y. He, S. Wong, and Y. Li, "Multifunctional vortex beam generation by a dynamic reflective metasurface," *Adv. Opt. Mater.*, vol. 9, no. 4, Feb. 2020, Art. no. 2001689.
- [18] M. Liu *et al.*, "Terahertz-field-induced insulator-to-metal transition in vanadium dioxide metasubstrates," *Nature*, vol. 487, no. 7407, pp. 345–348, Jul. 2012.
- [19] M. D. Goldflam *et al.*, "Voltage switching of a VO<sub>2</sub> memory metasurface using ionic gel," *Appl. Phys. Lett.*, vol. 105, no. 4, Jul. 2014, Art. no. 041117.
- [20] J. Jeong, A. Joushaghani, S. Paradis, D. Alain, and J. K. S. Poon, "Electrically controllable extraordinary optical transmission in gold gratings on vanadium dioxide," *Opt. Lett.*, vol. 40, no. 19, pp. 4408–4411, Oct. 2015.
- [21] H. Kocer *et al.*, "Thermal tuning of infrared resonant absorbers based on hybrid gold-VO<sub>2</sub> nanostructures," *Appl. Phys. Lett.*, vol. 106, no. 16, Apr. 2015, Art. no. 161104.
- [22] Z. M. Liu *et al.*, "A tunable metamaterial absorber based on VO<sub>2</sub>/W multilayer structure," *IEEE Photon. Technol. Lett.*, vol. 29, no. 22, pp. 1967–1970, Nov. 2017.
- [23] L. Lei, F. Lou, K. Tao, H. Huang, X. Cheng, and P. Xu, "Tunable and scalable broadband metamaterial absorber involving VO<sub>2</sub>-based phase transition," *Photon. Res.*, vol. 7, no. 7, pp. 734–741, Jul. 2019.
- [24] F. Fan, W. Gu, S. Chen, X. Wang, and S. Chang, "State conversion based on terahertz plasmonics with vanadium dioxide coating controlled by optical pumping," *Opt. Lett.*, vol. 38, no. 9, pp. 1582–1584, May 2013.
- [25] Y. Zhang *et al.*, "Photoinduced active terahertz metamaterials with nanosstructured vanadium dioxide film deposited by sol-gel method," *Opt. Exp.*, vol. 22, no. 9, pp. 11070–11078, May 2014.
- [26] X. Wang *et al.*, "Tunable Bragg filters with a phase transition material defect layer," *Opt. Exp.*, vol. 24, no. 18, pp. 20365–20372, Sep. 2016.
- [27] M. Sun *et al.*, "A photonic switch based on a hybrid combination of metallic nanoholes and phase-change vanadium dioxide," *Sci. Rep.*, vol. 8, Jul. 2018, Art. no. 11106.
- [28] M. Zhang and Z. Song, "Terahertz bifunctional absorber based on a graphene-spacer-vanadium dioxide-spacer-metal configuration," *Opt. Exp.*, vol. 28, no. 8, pp. 11780–11788, Apr. 2020.
- [29] Z. Che *et al.*, "Active controllable coded terahertz narrow bandpass filter based on vanadium dioxide," *Plasmonics*, vol. 16, no. 6, pp. 2269–2276, Jun. 2021.
- [30] Z. Xu and Z. Song, "VO<sub>2</sub>-based switchable metasurface with broadband photonic spin hall effect and absorption," *IEEE Photon. J.*, vol. 13, no. 4, Aug. 2021, Art. no. 4600305.
- [31] F. Ding, A. Pors, and S. I. Bozhevolnyi, "Gradient metasurfaces: A review of fundamentals and applications," *Rep. Prog. Phys.*, vol. 81, no. 2, Feb. 2018, Art. no. 026401.
- [32] J. Shabaniour, S. Beyraghi, and A. Cheldavi, "Ultrafast reprogrammable multifunctional vanadium-dioxide-assisted metasurface for dynamic THz wavefront engineering," *Sci. Rep.*, vol. 10, no. 1, Jun. 2020, Art. no. 8950.
- [33] R. Malureanu *et al.*, "A new method for obtaining transparent electrodes," *Opt. Exp.*, vol. 20, no. 20, pp. 22770–22782, Sep. 2012.
- [34] M. Naftaly and R. E. Miles, "Terahertz time-domain spectroscopy of silicate glasses and the relationship to material properties," *J. Appl. Phys.*, vol. 102, no. 4, Aug. 2007, Art. no. 043517.
- [35] Z. Song, Y. Deng, Y. Zhou, and Z. Liu, "Terahertz toroidal metasubstrates with tunable properties," *Opt. Exp.*, vol. 27, no. 4, pp. 5792–5797, Feb. 2019.
- [36] Y. Zhu, Y. Zhao, M. Holtz, Z. Fan, and A. A. Bernussi, "Effect of substrate orientation on terahertz optical transmission through VO<sub>2</sub> thin films and application to functional antireflection coatings," *J. Opt. Soc. Amer. B*, vol. 29, no. 9, pp. 2373–2378, Sep. 2012.
- [37] S. Wang, L. Kang, and D. H. Werner, "Hybrid resonators and highly tunable terahertz metasubstrates enabled by vanadium dioxide (VO<sub>2</sub>)," *Sci. Rep.*, vol. 7, Jun. 2017, Art. no. 4326.
- [38] F. Fan, W. H. Gu, S. Chen, X. H. Wang, and S. J. Chang, "State conversion based on terahertz plasmonics with vanadium dioxide coating controlled by optical pumping," *Opt. Lett.*, vol. 38, no. 9, pp. 1582–1584, May 2013.
- [39] U. K. Chettiar and N. Engheta, "Modeling vanadium dioxide phase transition due to continuous-wave optical signals," *Opt. Exp.*, vol. 23, no. 1, pp. 445–451, Jan. 2015.
- [40] S. L. Sun *et al.*, "High-efficiency broadband anomalous reflection by gradient meta-surfaces," *Nano Lett.*, vol. 12, no. 12, pp. 6223–6229, Dec. 2012.
- [41] S. Sun, Q. He, S. Xiao, Q. Xu, X. Li, and L. Zhou, "Gradient-index metasurfaces as a bridge linking propagating waves and surface waves," *Nature Mater.*, vol. 11, no. 5, pp. 426–431, May 2012.
- [42] L. Allen, M. W. Beijersbergen, R. J. C. Spreeuw, and J. P. Woerdman, "Orbital angular momentum of light and the transformation of Laguerre-Gaussian laser modes," *Phys. Rev. A*, vol. 45, no. 11, pp. 8185–8189, Jun. 1992.
- [43] F. Tamburini, E. Mari, A. Sponselli, B. Thide, A. Bianchini, and F. Romanato, "Encoding many channels on the same frequency through radio vorticity: First experimental test," *New J. Phys.*, vol. 14, Mar. 2012, Art. no. 033001.